






# Magnetospheric Multiscale Observations of Turbulence in the Magnetosheath on Kinetic Scales

W. M. Macek<sup>1,2,3</sup> , A. Krasínska<sup>2</sup>, M. V. D. Silveira<sup>3,4</sup>, D. G. Sibeck<sup>3</sup>, A. Wawrzaszek<sup>2</sup> , J. L. Burch<sup>5</sup>, and C. T. Russell<sup>6</sup> 

<sup>1</sup> Faculty of Mathematics and Natural Sciences, Cardinal Stefan Wyszyński University, Wóycickiego 1/3, 01-938 Warsaw, Poland; [macek@uksw.edu.pl](mailto:macek@uksw.edu.pl)

<sup>2</sup> Space Research Centre, Polish Academy of Sciences, Bartycka 18 A, 00-716 Warsaw, Poland; [akrasinska@cbk.waw.pl](mailto:akrasinska@cbk.waw.pl)

<sup>3</sup> NASA Goddard Space Flight Center, Code 6740, Greenbelt, MD 20771, USA; [david.g.sibeck@nasa.gov](mailto:david.g.sibeck@nasa.gov)

<sup>4</sup> Catholic University of America, Washington, DC 20064, USA; [marcosvinicius.diassilveira@nasa.gov](mailto:marcosvinicius.diassilveira@nasa.gov)

<sup>5</sup> Southwest Research Institute, San Antonio, TX, USA; [jburch@swri.edu](mailto:jburch@swri.edu)

<sup>6</sup> University of California, Los Angeles, 603 Charles Young Drive, Los Angeles, CA 90095-1567, USA; [crussell@igpp.ucla.edu](mailto:crussell@igpp.ucla.edu)

Received 2018 July 17; revised 2018 August 7; accepted 2018 August 10; published 2018 September 7

## Abstract

Our previous studies have produced phenomenological models for turbulence in solar wind plasmas on large- (inertial) magnetohydrodynamic scales, based on observations by the *Voyager*, *Ulysses*, and *THEMIS* missions. Here we consider turbulence in the Earth's magnetosheath, where timescales are often far shorter than those in the heliosheath, using observations from the currently operating *Magnetospheric Multiscale (MMS)* mission on much smaller kinetic scales. We employ a standard statistical analysis to obtain energy density spectra for the magnetic field strength and the ion speed at high time resolution. We find a clear breakpoint of the magnetic spectrum exponent from  $-0.8$  to  $-5/2$  near the ion gyrofrequency of 0.25 Hz. In fact, just behind the bow shock and near the magnetopause, the availability of the highest-resolution magnetic field observations enables us also to identify the expected spectral exponent of about  $-3$ , which is further followed by steeper spectra with the slopes from  $-7/2$  to  $-11/2$  ( $-16/3$ ) in the kinetic regime above 20 Hz, possibly resulting from the kinetic Alfvén waves. Because the resolution of the ion plasma parameters is somewhat lower than that for the magnetic field, spectra for the ion velocity can only be resolved near the onset of kinetic scales. On the other hand, deep inside the magnetosheath, where only low-resolution data are available and we are still in the magnetohydrodynamic scale range, we recover the well-known  $-5/3$  Kolmogorov's spectrum. The obtained results on kinetic scales may be useful for better understanding the physical mechanisms governing turbulence.

**Key words:** Earth – magnetic fields – methods: data analysis – plasmas – solar wind – turbulence

## 1. Introduction

Turbulence is a complex phenomenon that remains a challenge for contemporary science (Frisch 1995; Chang 2015). Notwithstanding great progress in magnetohydrodynamic (MHD; and Hall-MHD) turbulence simulations, the physical mechanisms for turbulence are still not clearly understood (Burlaga 1995; Biskamp 2003). Collisionless space and astrophysical plasmas can be considered natural laboratories for investigating the complex dynamics (e.g., Bruno & Carbone 2016). It is known that turbulent magnetic fields play an important role in our space environment, e.g., leading to magnetic reconnection (e.g., Burlaga 1995; Treumann 2009; Figura & Macek 2013) and the redistribution of kinetic and magnetic energy in space plasmas. The dynamic variability of these fields at small scales in the solar system is not well known. For example, reconnection processes may play an important role in mixing heliospheric and interstellar plasmas, as postulated by Macek & Grzedziński (1985), a hypothesis recently supported by numerical simulations (Strumik et al. 2013, 2014). Reconnection at the heliopause (the ultimate boundary separating the heliosphere from the very local interstellar plasma) has yet to be confirmed by experimental data.

Our previous studies employed an MHD approach to produce phenomenological models for turbulence in the solar wind plasma on relatively large scales in the inertial regime

based on *Voyager* deep-space mission observations of the outer heliosphere, including the heliosheath, and even the interstellar medium (Burlaga et al. 2013; Macek et al. 2014), on *Ulysses* spacecraft observations beyond the ecliptic plane (Wawrzaszek et al. 2015), and also on *THEMIS* mission observations of the Earth's magnetosheath (Macek et al. 2015, 2017, 2018).

Admittedly, the identification of turbulence scaling in the inertial range may not necessarily provide any specific physical mechanism for the multiple processes that are responsible for the distribution of energy or magnetic flux between cascading turbulent eddies. However, we are convinced that one must consider much smaller scales, where particle-wave interactions resulting in the dissipation of energy are effective (e.g., Alexandrova 2008; Yordanova et al. 2008). Hence, our basic research hypothesis is that small scales are essential for understanding the physical mechanisms of turbulence. In our view, it is necessary to investigate the experimental data at scale lengths below the inertial range. Based on the *Cluster* multi-spacecraft mission, Sahraoui et al. (2009) found a steepening of the power spectral density (PSD) on electron scales and confirmed the power-law spectrum with an exponent of  $-5/2$  (close to the expected  $-7/3$ ) between ion and electron scales (compare Sahraoui et al. 2013). On the other hand, analyzing mainly the *WIND* data Bruno et al. (2014) showed that the existence of a short frequency range, where the steepening is related to the PSD of fluid scales, is generally steeper than  $-7/3$ , and depends on the power density level of the fluctuations within the inertial range. Lion et al. (2016), Roberts et al. (2016), and Perrone et al. (2016, 2017) have



Original content from this work may be used under the terms of the [Creative Commons Attribution 3.0 licence](https://creativecommons.org/licenses/by/3.0/). Any further distribution of this work must maintain attribution to the author(s) and the title of the work, journal citation and DOI.

further investigated the nature of solar wind magnetic fluctuations on ion scales based on the missions.

Yordanova et al. (2016) reported *Magnetospheric Multiscale* (*MMS*) observations of electron scale current sheets in the turbulent magnetosheath behind the quasi-parallel shock. Chasapis et al. (2017) have analyzed high-order structure functions using both *MMS* and *Cluster* data. Breuillard et al. (2018) recently analyzed the spectral properties of the magnetosheath downstream of the quasi-parallel and quasi-perpendicular bow shocks, suggesting that the high-resolution *MMS* data can provide better insight into the nature of turbulence in the magnetosheath at ion and electron kinetic scales. However, the dependence of the spectrum on the location in the magnetosheath with different available data resolutions has not yet been explored. Moreover, we are convinced that the gross features of turbulence should still be determined by Alfvén waves (e.g., Belcher & Davis 1971), involving the magnetic field and the ion bulk speed of the plasma, possibly related to discontinuities (Borovsky 2010), current sheets, mirror mode structures, or instabilities (Tsurutani et al. 2011).

Therefore, this Letter focuses on the transition from MHD to ion scales for both high- and low-resolution *MMS* data, which still needs further investigation. Following our previous study based on the *THEMIS* data (Macek et al. 2015, 2017), we analyze in fuller detail turbulence on sub-ion scales in the entire magnetosheath region depending on highly variable plasma, in order to compare the characteristics of turbulence spectra, when going from the MHD to kinetic scales. This leads to a description of space plasmas within kinetic theory, instead of an MHD approach.

In particular, we have confirmed a clear breakpoint in the magnetic energy spectra, which occurs near the ion gyrofrequencies behind the bow shock, inside the magnetosheath, and before leaving the magnetosheath. We have also observed that the spectrum steepens at these points to power exponents in the kinetic range from  $-5/2$  to  $-11/2$  for the magnetic field data of the highest resolution available within the *MMS* mission. The high- and low-resolution data used in our study are described in Section 2. The obtained characteristic plasma parameters, together with the magnetic and plasma spectra, are presented in Section 3. Finally, the importance of turbulence on the sub-ion scales for astrophysical plasmas is summarized in Section 4.

## 2. Data

The *MMS* mission was launched in 2015 to investigate magnetic reconnection near the Earth’s magnetopause and in the magnetotail (Burch et al. 2016). This Letter investigates magnetosheath turbulence (a) just behind the bow shock (BS), (b) inside the magnetosheath (SH), and (c) near the magnetopause (MP). Figure 1 shows the *MMS* 1 trajectory in the Geocentric Solar Ecliptic (GSE) coordinates. The dotted–dashed line shows the position of the bow shock (Wu et al. 2000), while the solid line shows the magnetopause (Shue et al. 1998). Table 1 lists the respective time intervals. The local angle  $\theta_{\text{Bn}}$  between the normal  $\mathbf{n}$  (at the bow shock nose) to the surface of the shock and the direction of the ambient magnetic field  $\mathbf{B}$  is estimated to indicate whether the magnetosheath lies behind the quasi-parallel ( $0^\circ \leq \theta_{\text{Bn}} \leq 45^\circ$ ) or quasi-perpendicular ( $45^\circ < \theta_{\text{Bn}} \leq 90^\circ$ ) shock (e.g., Leroy 1983); here we have the intermediate type of shocks.

For the magnetic field strength  $B = |\mathbf{B}|$ , we use BURST file data from the FluxGate Magnetometers (FGM; Russell et al. 2016) with the highest resolution of 7.8 ms, and survey data with substantially lower time resolutions of 0.0625–0.125 s. All

of the data are available from <http://cdaweb.gsfc.nasa.gov>. For the ion plasma velocity  $V = |\mathbf{V}|$  we use observations measured by the Dual Ions Spectrometer instrument (DIS; Pollock et al. 2016), with somewhat lower time resolution; namely, in the BURST type we have 150 ms for ions (Dual Electron Spectrometer (DES) provides 30 ms for electrons). In FAST Mode the instruments provide moments each 4.5 s. Using the highest-resolution data available for the selected bow shock interval (a) lasting 5 minutes, there are 37,856 measurement points for the magnetic field and 1973 points for the plasma bulk velocity. For case (b), deep inside the magnetosheath between the bow shock and the magnetopause, only the low-resolution data are available, representing averages of the BURST data. Despite this, we have found a long interval of 3.5 hr consisting of 198,717 points for  $B$  and 2760 points for  $V$ . Near the magnetopause, case (c), the highest-resolution data are again available and even for a rather short interval of about 1.8 minutes, we still have 13,959 measurement points for the magnetic field and 733 points for the ion velocity.

## 3. Results

The lagged solar wind conditions governing the cases under study are given in the last three columns of Table 1, which have been calculated using the omnidirectional (OMNI) data (available from [omniweb.gsfc.nasa.gov](http://omniweb.gsfc.nasa.gov)), for a location just downstream the bow shock (case (a)), for turbulence inside the magnetosheath (case (b)), and finally just outside the magnetopause (case (c)).

The Alfvén Mach numbers  $M_A$  are defined here as the ratio ( $V/V_A$ ) of the ion velocity  $V$  to the Alfvén velocity  $V_A = B/(\mu_0\rho)^{1/2}$ , where  $\rho = mN$  is the mass density for ions of mass  $m$  and the number density  $N$  ( $\mu_0$  denotes the permeability of free space), assuming the standard solar wind composition (95% of hydrogen and 5% of helium) ions (with  $m = 1.15 m_p$ , the proton mass). The calculated values of the Alfvén Mach numbers, which can be considered as a strength of the shock itself, are rather high, ranging from 13 to 20. The ratio of the solar wind thermal pressure to the magnetic pressure, i.e., the plasma parameter  $\beta$  from 2 to 5, as given by  $p/(B^2/(2\mu_0\rho))$ , indicates that the thermal pressure dominates the magnetic pressure. The magnetosonic Mach number  $M_{\text{ms}}$ , which is the ratio of the velocity to the magnetosonic velocity,  $V_{\text{ms}} = \sqrt{V_A^2 + V_S^2}$ , where the sonic speed is  $V_S = \sqrt{\gamma p/\rho}$  ( $\gamma = 5/3$  is the polytropic index), is similar in all of these cases; for a more detailed analysis on shock parameters, see the review by Macek et al. (2018).

The magnetosheath can easily be identified on the basis of broad ion energy spectra ranging from 100 eV to a few keV as illustrated for each sample in the upper panels of Figures 2–4, respectively. The second and third panels show the magnetic field strength  $|\mathbf{B}|$  and the ion velocity  $|\mathbf{V}|$ . The fourth panel presents the ion and electron temperatures perpendicular to the local magnetic field  $\mathbf{B}$ , i.e.,  $T_{\perp i}$  and  $T_{\perp e}$ . The fifth and sixth panels show the calculated ion and electron gyrofrequencies,  $f_{ci}$  and  $f_{ce}$ , which characterize the kinetic regime, with averages shown by dashed lines.

At the bottom of Figures 2–4 we present the magnetic and plasma kinetic energy density spectra obtained using the Welch (1967) method, for the cases listed in Table 1. Consider the spectrum obtained just behind crossing the bow shock shown in Figure 2. Taking the mean magnetic field strength in this interval  $B = 18.85$  nT, we obtain average ion and electron gyrofrequencies of  $f_{ci} = 0.25$  Hz and  $f_{ce} = 528$  Hz, respectively. Further, with

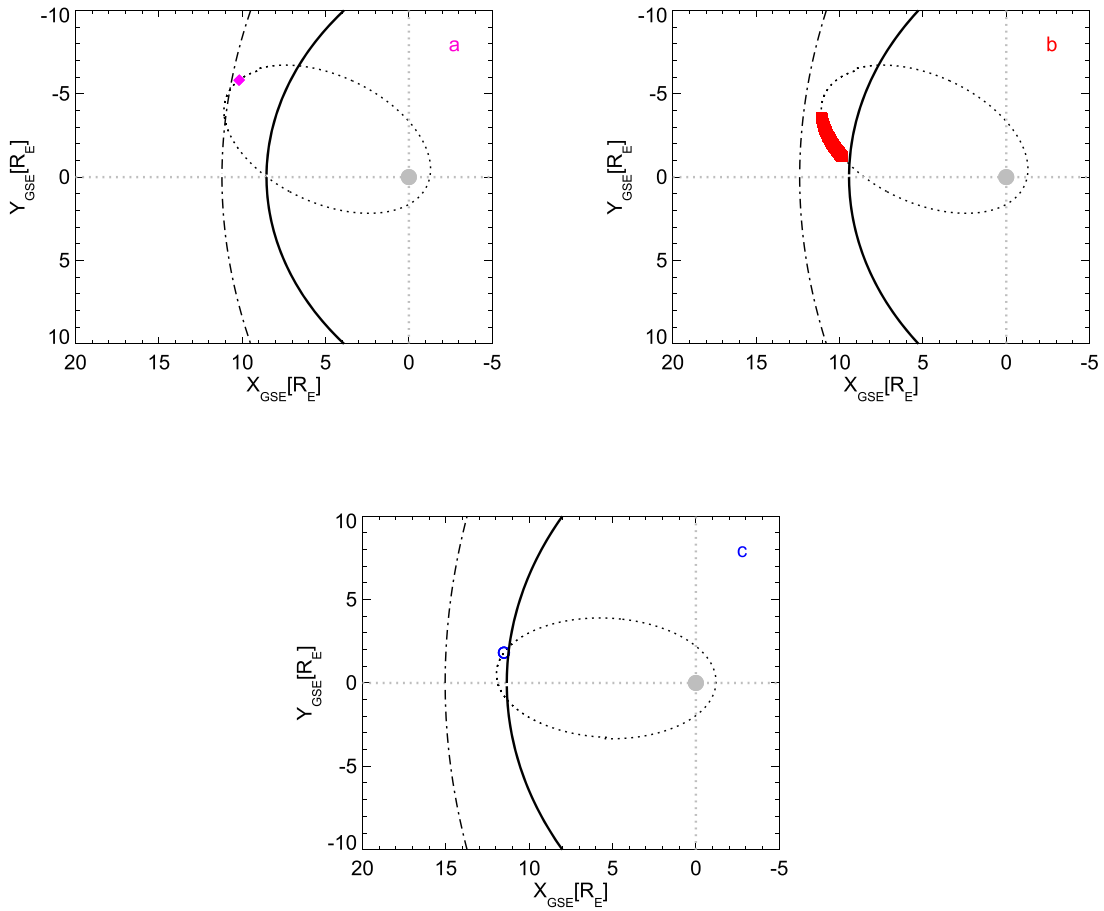


**Figure 1.** *MMS 1* spacecraft trajectory in the magnetosheath: (a) behind the bow shock, (b) inside the magnetosheath, and (c) near the magnetopause.

**Table 1**  
List of Selected *MMS 1* Interval Samples (hh.min:ss)

Case	Resolution	Time (y.m.d)	Location	Begin	End	$\theta_{Bn}$ ( $^\circ$ )	$M_A$	$\beta$	$M_{ms}$
(a)	High	2015.12.28	BS	01.48:04	01.52:59	$35.8 \pm 7$	19.3	4.5	8.7
(b)	Low	2015.12.28	SH	06.19:00	09.45:59	$46.6 \pm 21$	19.9	4.9	8.7
(c)	High	2016.12.27	MP	11.30:24	11.32:13	$32.0 \pm 13$	12.8	2.2	7.5

the mean ion temperature perpendicular to  $\mathbf{B}$  of  $T_{\perp i} \approx 420$  eV, we calculate the mean Larmor radius for ions to be  $r_{Li} = 119$  km  $\sim 100$  km. Similarly, with the mean electron perpendicular temperature  $T_{\perp e} \approx 46$  eV, we have obtained the respective electron Larmor radius to be  $r_{Le} = 0.86$  km, of the order of 1 km. This means that kinetic scales, estimated using the Taylor (1938) hypothesis, should approximately span the interval from 1 to 100 km.

In addition, taking the average ion number density in the interval  $n_i = 27.47$  cm $^{-3}$ , and the corresponding ion plasma (angular) frequency ( $\omega_p = 2\pi f_p$ ), we calculate the ion inertial length ( $c$  denotes the speed of light),  $\lambda_i = c/(\omega_{pi}) = 46.65$  km. Similarly, with the average electron density  $n_e = 25.44$  cm $^{-3}$ , the electron inertial length (plasma skin depth) is  $\lambda_e = c/(\omega_{pe}) = 1.05$  km, i.e., basically of the same order as the electron gyroradius  $r_{Le}$ . Therefore, employing the Taylor's hypothesis (using the average velocity of the solar wind flow in the magnetosheath,  $V$ , in the third panel of Figure 2), we estimate the characteristic frequency  $\omega_\lambda = 2\pi f_\lambda = (V/c) \omega_p$  for ions  $f_{\lambda i} = 0.55$  Hz and electrons

$f_{\lambda e} = 24.5$  Hz, respectively, see (e.g., Leamon et al. 1998). The vertical dashed line in the spectra presented in Figures 2–4 displays the ion gyrofrequency  $f_{ci}$  (we are well below the electron gyrofrequency  $f_{ce}$ ) and the dashed–dotted and dotted lines denote the characteristic ion  $f_{\lambda i}$  and electron  $f_{\lambda e}$  frequencies related to the respective inertial scales estimated using the Taylor's hypothesis.

Thanks to the high-resolution observations available for the magnetic field, we obtain a spectral exponent of  $-2.6 \pm 0.1$  ( $\approx -5/2$ ) for the magnetic energy density spectrum when entering the kinetic regime, which is clearly steeper than the standard Kolmogorov- (1941) ( $-5/3$ ) or Kraichnan- (1965) ( $-3/2$ ) type spectrum, characteristic for the inertial region of magnetized plasma (compare Salem et al. 2009). As can be seen, the spectrum begins near the ion gyrofrequency,  $f_{ci} \sim 0.25$  Hz (close to  $f_{\lambda i} \sim 0.55$  Hz, as is observed here in the frequency range from  $\sim 10^{-1}$  Hz), and ends near the Taylor-shifted frequency  $f_{\lambda e} \sim 25$  Hz, corresponding to the electron inertial length, marked by the vertical dashed and dotted lines, i.e., far below the electron gyrofrequency,  $f_{ce} \approx 528$  Hz (not shown

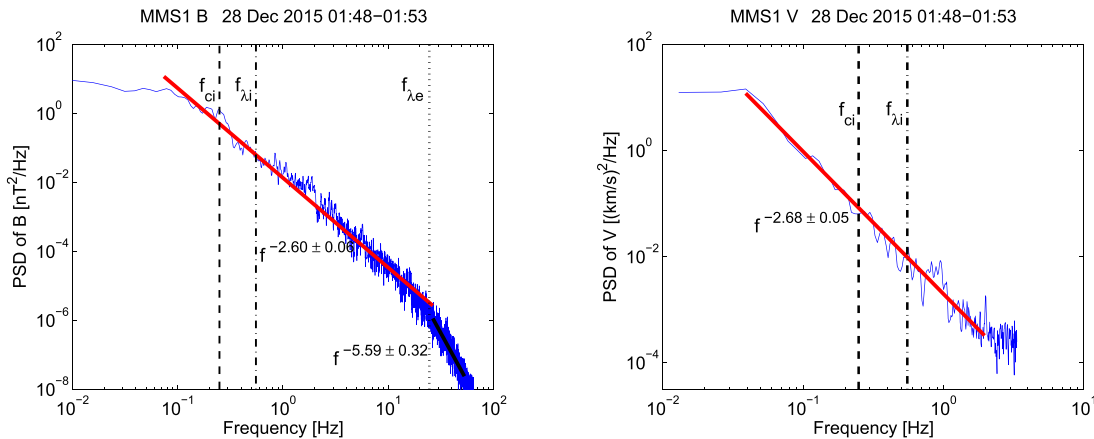
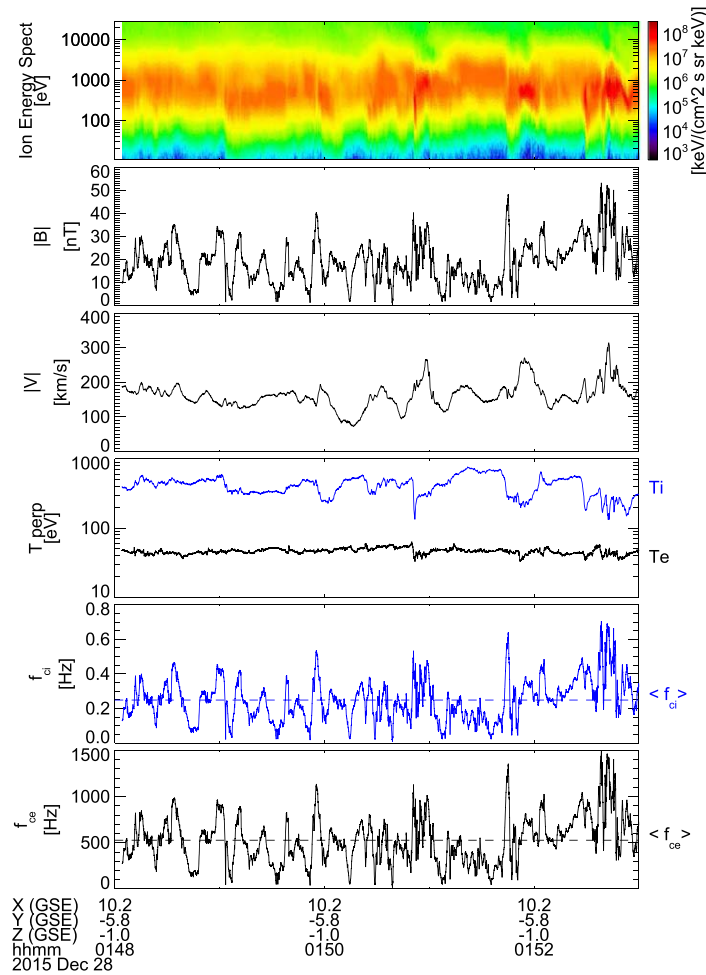


**Figure 2.** High-resolution turbulence in the magnetosheath near the bow shock (BS), case (a) in Table 1, for frequencies above the ion gyrofrequency  $f_{ci}$  marked by the dashed vertical line, and between the ion  $f_{Li}$  and electron  $f_{Le}$  Taylor-shifted inertial frequencies shown by the dashed-dotted and dotted lines, respectively.

here). Therefore, it is worth noting that above the electron inertial scale this is further followed by an even steeper spectrum with the slope of  $-5.59 \pm 0.32$  (close to  $-11/2$  or  $-16/3$ ). Because the resolution for the ion plasma parameters is only of 150 ms, a spectral exponent of  $-2.68 \pm 0.05$  for the energy density related to the magnitude of the ion velocity  $V$  (similar to that for the magnetic spectrum above  $f_{ci}$ ) can only be resolved between 0.04 and 2 Hz, namely only near the onset of kinetic scales.

Figure 3 presents observations within the mid-magnetosheath. As noted earlier, in Section 2, only lower-resolution data are available here. Using a very long sample of about 3.5 hr we can obtain spectra, and the characteristic plasma parameters can be well established in this region. Taking the mean magnetic field strength in this interval  $B = 18.23$  nT, we obtain on the average  $f_{ci} = 0.24$  Hz,  $f_{ce} = 510$  Hz. Further, with  $T_{\perp i} \approx 392$  eV, we calculate ion gyroscale  $r_{Li} = 119$  km.

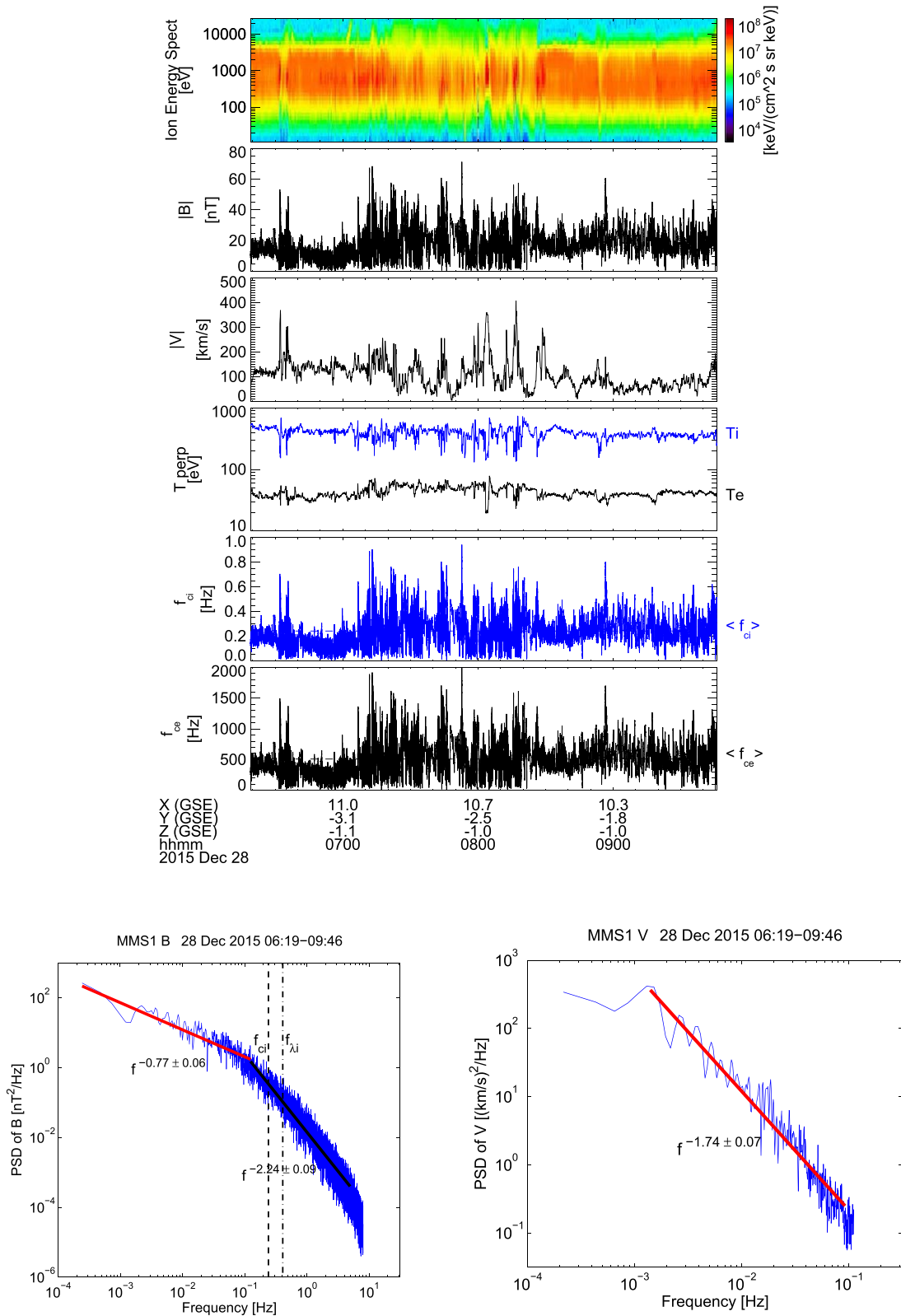


**Figure 3.** Low-resolution turbulence inside the magnetosheath (SH), case (b) in Table 1, for frequencies below and above the ion gyrofrequency  $f_{ci}$  and the ion Taylor-shifted inertial scale frequency  $f_{\lambda_i}$  marked by the vertical dashed and dashed-dotted lines, respectively.

Similarly, with  $T_{\perp e} \approx 43$  eV, the respective scale of electron,  $r_{Le} = 0.85$  km, is again of the order of 1 km. Here with  $n_i = 34.97 \text{ cm}^{-3}$  and  $n_e = 32.20 \text{ cm}^{-3}$  the ions and electron inertial lengths are  $\lambda_i = 41$  km and  $\lambda_e = 0.94$  km, similar to

case (a), Figure 2. The same applies for the Taylor's shifted values  $f_{\lambda_i} = 0.41$  Hz and  $f_{\lambda_e} = 18.1$  Hz.

It is interesting to see at the bottom of Figure 3 a clear break in the slope of the magnetic spectra from  $-0.77 \pm 0.06$  to



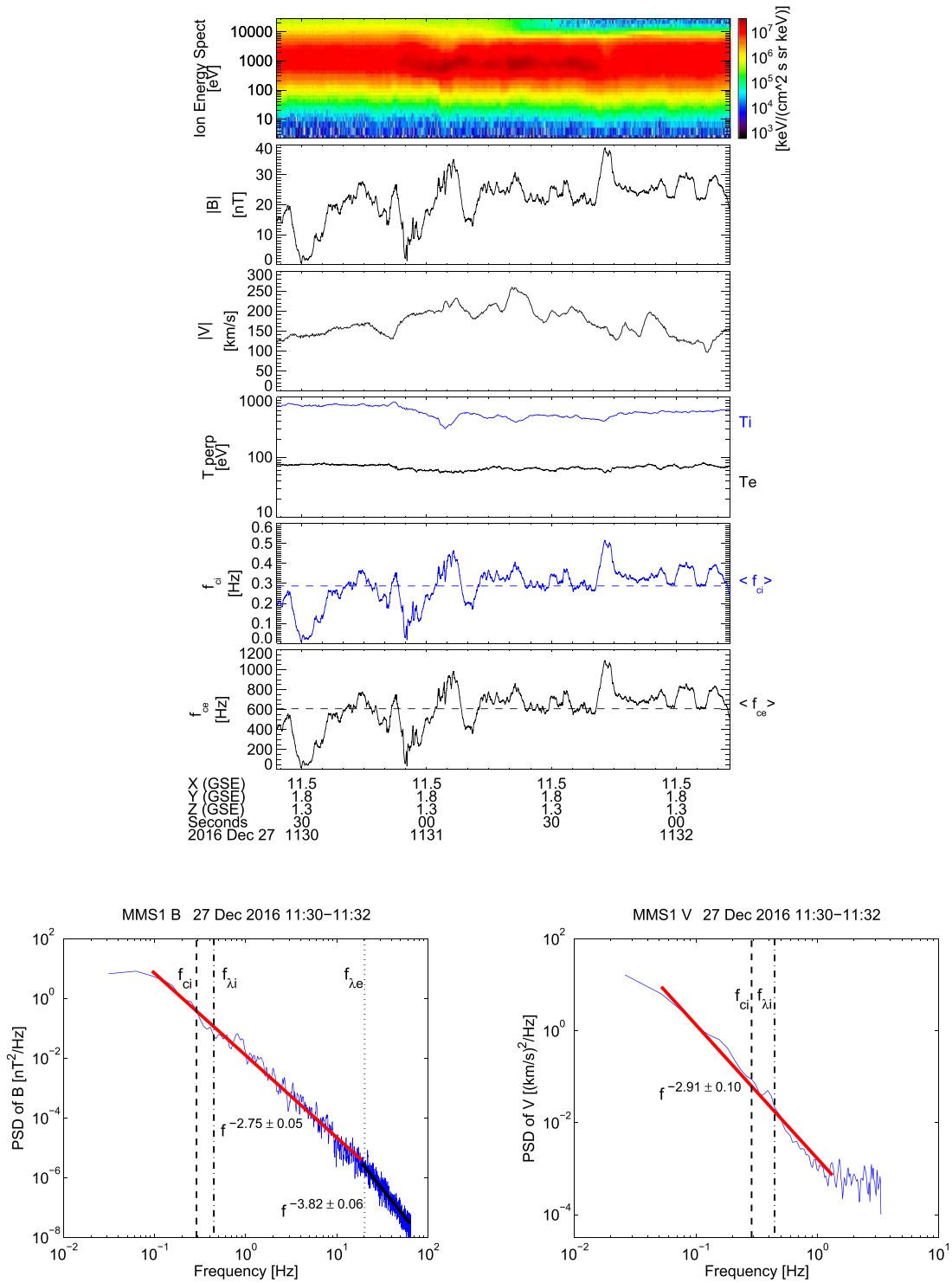


**Figure 4.** High-resolution turbulence near the magnetopause (MP), case (c) in Table 1, for frequencies above the ion gyrofrequency  $f_{ci}$  marked by the dashed vertical line, and between the ion  $f_{\lambda_i}$  and electron  $f_{\lambda_e}$  Taylor-shifted inertial scale frequencies shown by the dashed-dotted and dotted lines, respectively.

$-2.24 \pm 0.09$ , which is consistent with a somewhat similar recent analysis of the Alfvénic fluctuations by Breuillard et al. (2018). In Figure 3 the breakpoint lies at 0.12 Hz, i.e., near the ion gyrofrequency  $f_{ci} = 0.24$  Hz, and still close to the ion inertial scale,  $f_{\lambda_i} = 0.41$  Hz, followed by a steeper power law with the slope of  $-5/2$  (observed here till several Hz only). Behind the quasi-parallel shocks, Breuillard et al. (2018) also found an additional power law observed in between (0.02 and 0.2 Hz), i.e., in the inertial regime, with a spectral index of about  $-1.6$ . Here we are interested in the

transition from the MHD to kinetic scales, but in the case of a shock that is more quasi-perpendicular ( $\theta_{Bn} = 47^\circ$ ), because of the lower-resolution data available for the plasma velocity  $|V|$ , we can still recover a spectral exponent of  $-1.74 \pm 0.07$  between  $10^{-3}$  and  $10^{-1}$  Hz, this means in the MHD scale range (i.e., below  $f_{ci}$  and  $f_{\lambda_{i,e}}$ , not seen in this spectrum), which seems also to be close to the Kolmogorov (1941) type with the well-known exponent of  $-5/3$ .

Fortunately, the high-resolution observations are available near the magnetopause. Taking  $B = 21.75$  nT, we obtain the average

parameters  $f_{ci} = 0.29$  Hz and  $f_{ce} = 609$  Hz. Now, with  $T_{Li} \approx 574$  eV, we calculate  $r_{Li} = 120.5$  km, and similarly, with  $T_{Le} \approx 68$  eV, we have obtained the respective scale of electron  $r_{Le} = 0.9$  km. In this case we have on the average  $n_i \approx 16.16$  cm<sup>-3</sup> and  $n_e \approx 15.56$  cm<sup>-3</sup> resulting in characteristic frequencies related to the respective inertial lengths  $\lambda_i = 61$  km and  $\lambda_e = 1.35$  km, and the Taylor's shifted values  $f_{\lambda_i} = 0.45$  Hz and  $f_{\lambda_e} = 20.1$  Hz, similar to that for the previous cases under our study.

In addition to the parameters characteristic for kinetic scales, as already discussed for cases (a) and (b) in Figures 2 and 3, now for case (c) Figure 4 shows a slope exponent of  $-2.75 \pm 0.05$ , above the ion gyrofrequency of about 0.3 Hz and the Taylor-shifted ion frequency of 0.45 Hz, and above the electron inertial scale of 20 Hz followed by steeper spectrum with the slope of  $-3.82 \pm 0.06$  (close to  $-7/2$ ). Similar slopes for velocity can only be resolved between 0.04 and 3.5 Hz, near the onset of kinetic scales. We see that the obtained power law fitted to the high-resolution *MMS* data is characteristic for the kinetic regime in both the magnetic field and plasma velocity measurements (compare Sahraoui et al. 2013, Figure 4), which is also consistent with the very recent results obtained by Breuillard et al. (2018). A detailed analysis of turbulence in the magnetosheath based on the high-resolution *MMS* plasma and magnetic field data by using the Elsässer variables, similar to that for *THEMIS* (Macek et al. 2017), will be presented in a more comprehensive study in the near future.

#### 4. Conclusions

We have looked at turbulence spectra in regions behind the bow shock and close to the magnetopause, using the highest-resolution data, and also deep inside the magnetosheath, where only lower-resolution data are available. However, in this case, near the ion frequency of 0.25 Hz, we have observed a clear change of the spectral exponent of the magnetic spectra from  $-0.8$  to much steeper spectrum with the slope of  $-5/2$ , which is substantially different than that for the standard Kolmogorov (1941) or Kraichnan (1965) spectra with the slope of  $-5/3$  or  $-3/2$ , characteristic for an inertial region in the magnetized plasma.

Moreover, just behind the bow shock and also near the magnetopause, the availability of the high-resolution magnetic field data of 7.8 ms enabled us to observe a spectral exponents in the kinetic regime (here between 0.1 and about 65 Hz) from  $-5/2$  above the ion gyrofrequency till  $-7/2$  or even  $-11/2$  (or  $-16/3$ ) above the Taylor-shifted frequency related to the electron skin depth of above say 20–25 Hz, which could result from the dissipation of the kinetic Alfvén waves (e.g., Schekochihin et al. 2009). Because the plasma resolution for ions is only 150 ms, the similar spectrum for the velocity can only be resolved between 0.04 and 3.5 Hz, near the onset of kinetic scales, which is at least inside the magnetosheath similar to the Kolmogorov (1941) type with the well-known slope of  $-5/3$ .

Hence, in view of the current and forthcoming space investigations, we expect that our study on the difference in characteristic of energy spectral density can facilitate a better understanding of the physical processes after applying kinetic theory for turbulence in various regions of space and astrophysical plasmas.

We are grateful for the dedicated efforts of the entire *MMS* mission team, including development, science operations, and the Science Data Center at the University of Colorado. We especially benefited from the efforts of T. E. Moore as a Project Scientist and C. J. Pollock for providing the data

that are available online from <http://cdaweb.gsfc.nasa.gov>. We acknowledge M. L. Adrian, Deputy Project Scientist, for discussion on the field and plasma instruments. This work has been supported by the National Science Center, Poland (NCN), through grant 2014/15/B/ST9/04782, and from the *MMS* project through the Catholic University of America during a visit by W.M.M to the NASA Goddard Space Flight Center.

#### ORCID iDs

W. M. Macek  <https://orcid.org/0000-0002-8190-4620>  
A. Wawrzaszek  <https://orcid.org/0000-0001-9946-3547>  
C. T. Russell  <https://orcid.org/0000-0003-1639-8298>

#### References

- Alexandrova, O. 2008, *NPGeo*, **15**, 95  
Belcher, J. W., & Davis, L. J. 1971, *JGR*, **76**, 3534  
Biskamp, D. 2003, *Magnetohydrodynamic Turbulence* (Cambridge: Cambridge Univ. Press)  
Borovsky, J. E. 2010, *PhRvL*, **105**, 111102  
Breuillard, H., Matteini, L., Argall, M. R., et al. 2018, *ApJ*, **859**, 127  
Bruno, R., & Carbone, V. 2016, *Turbulence in the Solar Wind*, Vol. 928 (Berlin: Springer)  
Bruno, R., Trenchi, L., & Telloni, D. 2014, *ApJL*, **793**, L15  
Burch, J. L., Moore, T. E., Torbert, R. B., & Giles, B. L. 2016, *SSRv*, **199**, 5  
Burlaga, L. F. 1995, *Interplanetary Magnetohydrodynamics* (New York: Oxford Univ. Press)  
Burlaga, L. F., Ness, N. F., & Stone, E. C. 2013, *Sci*, **341**, 147  
Chang, T. T. S. 2015, *An Introduction to Space Plasma Complexity* (Cambridge: Cambridge Univ. Press)  
Chasapis, A., Matthaeus, W. H., Parashar, T. N., et al. 2017, *ApJL*, **844**, L9  
Figura, P., & Macek, W. M. 2013, *AnPhy*, **333**, 127  
Frisch, U. 1995, *Turbulence. The Legacy of A.N. Kolmogorov* (Cambridge: Cambridge Univ. Press)  
Kolmogorov, A. 1941, *DoSSR*, **30**, 301  
Kraichnan, R. H. 1965, *PhFl*, **8**, 1385  
Leamon, R. J., Smith, C. W., Ness, N. F., Matthaeus, W. H., & Wong, H. K. 1998, *JGR*, **103**, 4775  
Leroy, M. M. 1983, *PhFl*, **26**, 2742  
Lion, S., Alexandrova, O., & Zaslavsky, A. 2016, *ApJ*, **824**, 47  
Macek, W., & Grzedzielski, S. 1985, in *Twenty Years of Plasma Physics*, ed. B. McNamara (Singapore: World Scientific), 320  
Macek, W. M., Wawrzaszek, A., & Burlaga, L. F. 2014, *ApJL*, **793**, L30  
Macek, W. M., Wawrzaszek, A., & Kucharuk, B. 2018, *NPGeo*, **25**, 39  
Macek, W. M., Wawrzaszek, A., Kucharuk, B., & Sibeck, D. G. 2017, *ApJL*, **851**, L42  
Macek, W. M., Wawrzaszek, A., & Sibeck, D. G. 2015, *JGRA*, **120**, 7466  
Perrone, D., Alexandrova, O., Mangeney, A., et al. 2016, *ApJ*, **826**, 196  
Perrone, D., Alexandrova, O., Roberts, O. W., et al. 2017, *ApJ*, **849**, 49  
Pollock, C., Moore, T., Jacques, A., et al. 2016, *SSRv*, **199**, 331  
Roberts, O. W., Li, X., Alexandrova, O., & Li, B. 2016, *JGRA*, **121**, 3870  
Russell, C. T., Anderson, B. J., Baumjohann, W., et al. 2016, *SSRv*, **199**, 189  
Sahraoui, F., Goldstein, M. L., Robert, P., & Khotyaintsev, Y. V. 2009, *PhRvL*, **102**, 231102  
Sahraoui, F., Huang, S. Y., Belmont, G., et al. 2013, *ApJ*, **777**, 15  
Salem, C., Mangeney, A., Bale, S. D., & Veltri, P. 2009, *ApJ*, **702**, 537  
Schekochihin, A. A., Cowley, S. C., Dorland, W., et al. 2009, *ApJS*, **182**, 310  
Shue, J.-H., Song, P., Russell, C. T., et al. 1998, *JGR*, **103**, 17691  
Strumik, M., Czechowski, A., Grzedzielski, S., Macek, W. M., & Ratkiewicz, R. 2013, *ApJL*, **773**, L23  
Strumik, M., Grzedzielski, S., Czechowski, A., Macek, W. M., & Ratkiewicz, R. 2014, *ApJL*, **782**, L7  
Taylor, G. I. 1938, *RSPSA*, **164**, 476  
Treumann, R. A. 2009, *A&ARv*, **17**, 409  
Tsurutani, B. T., Lakhina, G. S., Verkhoglyadova, O. P., et al. 2011, *JGRA*, **116**, A02103  
Wawrzaszek, A., Echim, M., Macek, W. M., & Bruno, R. 2015, *ApJL*, **814**, L19  
Welch, P. D. 1967, *IEEE Trans. Audio Electroacoust.*, **15**, 70  
Wu, D. J., Chao, J. K., & Lepping, R. P. 2000, *JGR*, **105**, 12627  
Yordanova, E., Vaivads, A., André, M., Buchert, S. C., & Vörös, Z. 2008, *PhRvL*, **100**, 205003  
Yordanova, E., Vörös, Z., Varsani, A., et al. 2016, *GeoRL*, **43**, 5969